Ultrahigh β-phase content poly(vinylidene fluoride) with relaxor-like ferroelectricity for high energy density capacitors

Nan Meng, Xintong Ren, Giovanni Santagiuliana, Leonardo Ventura, Han Zhang, Jiyue Wu, Haixue Yan, Michael J Reece, Emiliano Bilotti*

School of Engineering and Materials Science, Queen Mary University of London, Mile End Road, E1 4NS, UK
E-mail: e.bilotti@qmul.ac.uk

Abstract

Poly(vinylidene fluoride)-based dielectric materials are prospective candidates for electric high power density energy storage applications because of their ferroelectric nature, high dielectric breakdown strength and superior processability. However, obtaining a polar phase with relaxor-like behavior in poly(vinylidene fluoride), as required for high energy storage density, is a major challenge. To date, this has been achieved using complex and expensive synthesis of copolymers and terpolymers or via irradiation with high-energy electron-beam or γ-ray radiations. Herein, a facile process of pressing-and-folding is proposed to produce β-poly(vinylidene fluoride) (β-phase content: ~ 98%) with relaxor-like behavior observed in poly(vinylidene fluoride) with high molecular weight > 534 kg mol^{-1}, without the need of any hazardous gases, solvents, electrical or chemical treatments. ~~This simple and scalable processing route generates unprecedentedly high β-phase content (~98%) and relaxor-like behavior in poly(vinylidene fluoride) with high molecular weights (>534 kg mol^{-1}).~~ An ultra-high energy density (35 J cm^{-3}) with a high efficiency (74%) is achieved in a pressed-and-folded poly(vinylidene fluoride) (670-700 kg mol^{-1}), which is the highest value ever reported for a polymer-based dielectric capacitor.

Introduction

The demands of reducing both CO_2 emissions and the consumption of fossil fuels require an enhancement of the efficiency of energy usage and the long-term pursuit of renewable and sustainable energy sources (such as solar, wind, wave, etc.). These energy sources are intermittent, and it is therefore of paramount importance to develop efficient, low-cost and environmentally friendly electric energy storage systems. Currently there are three main options: batteries, electrochemical capacitors and dielectric capacitors.[1] Batteries, with their high energy density (lead-acid battery: 200-400 J cm^{-3} and lithium ion: 900-2500 J cm^{-3}) and low power density (<500 W kg^{-1}), are usually used for applications which require relatively slow release of energy (>100 s), while capacitors, with their high power density (electrochemical capacitors: 10^1-10^6 W kg^{-1} and dielectric capacitors: ~10^8 W kg^{-1}), are used for instant release of energy (<0.01 s).[2] Electrochemical capacitors have at least an order of magnitude higher energy density compared to dielectric capacitors but suffer from lower power density and lower output voltage. Only dielectric capacitors can meet the requirement of ultrahigh power density (up to ~10^8 W kg^{-1})[1], with the added benefits of long service life and fast release of energy,[3] which makes them important for high power/pulse power technologies, such as motor drives, mobile power system, space-vehicle power systems, electrochemical guns, *etc.*[4, 5]

However, the application of dielectric capacitors is currently limited by their low energy density, especially in applications requiring large capacitances and small packaging size. For example, the best performing commercial dielectric capacitor, biaxially-oriented polypropylene (BOPP), only has an energy density of ~1-2 J cm^{-3}, being an order of magnitude lower compared to commercial electrochemical capacitors (20-29 J cm^{-3}).[6, 7] Therefore, achieving high energy density in dielectric capacitors is a major bottleneck in extending their practical applications. The recoverable energy storage (U_{rec}) for dielectric capacitors is generally described by the following equation: $U_{rec} = \int E \mathrm{d}D$, where E and D are electric field and displacement,

respectively. Specifically, for linear dielectrics, $U_{\text{rec}} = \int E dD = \frac{1}{2} DE = \frac{1}{2} \varepsilon_0 \varepsilon_r {E_b}^2$, where ε_0 and

ε_r are the vacuum and relative dielectric constant, respectively, and E_b is the breakdown field.

U_{rec} has a quadratic-dependence on E_b. While polymers possess much lower dielectric constants

compared to inorganic materials, they have at least an order of magnitude higher energy storage

capacity as a result of their much higher breakdown fields (several hundred of kV mm^{-1}). Apart

from their high E_b, polymers have additional advantages, like low density, high processability,

mechanical flexibility and high toughness.

The relatively low ε_r of polymers is the limiting factor for their U_{rec}. The above

mentioned BOPP, for instance, has a ε_r of ~2. Polar polymers, with dipole moments in their

polymer chains, can exhibit much higher ε_r. Poly(vinylidene fluoride) (PVDF) is a typical

example[8, 9, 10] with a ε_r of ~10. PVDF has at least four well-defined phases, α-, β-, γ- and δ-

phase. The α-phase is non-polar, while the other three are polar phases, of which the β-phase

shows the highest polarization and the most favourable ferroelectric properties.[11, 12, 13, 14]

However, PVDF crystallizes predominantly into α-phase from the melt, with fairly low content

of β-phase (<8%),[15] which can be increased by solid-state drawing and/or high electric field

poling (~50-85%).[16] β-PVDF exhibits broad ferroelectric hysteresis loops and is not suitable

for energy storage (**Supplementary Figure 1**).[17] Relaxor (RFE) or anti-ferroelectric (AFE)

behaviour is instead desirable for energy storage (Supplementary Figure 1).[17] But RFE or AFE

behaviour have only been reported in the case of electron- or γ-irradiated

poly(vinylidenefluoride-trifluoroethylene)   P(VDF-TrFE),[18]   ternary   polymers

poly(vinylidenefluoride-trifluoroethylene-chlorofluoroethylene) P(VDF-TrFE-CFE)[19] and

poly(vinylidenefluoride-trifluoroethylene-chlorotrifluoroethylene P(VDF-TrFE-CTFE)[20] and

PVDF-based graft polymers such as P(VDF-CTFE)-*graft*-polystyrene.[21] The complexity and

cost of the above polymers and processes present a major barrier to their commercial use.

Our work focuses on virgin, commercially available and inexpensive PVDF homo-polymers, and demonstrates a facile and scalable processing route to obtain an ultrahigh content of β-phase (~98% of crystalline phase) with RFE-like behaviour that has an exceptionally high energy storage density of 35 J cm^{-3}, which is achieved by reversible field-induced transitions related to thermally unstable local polar structures. This is the highest value ever reported for a polymer-based dielectric material (**Supplementary Table 1**)[22, 23, 24, 25, 26, 27, 28, 29, 30, 31], to the best of our knowledge. The produced homo-polymer PVDF films show the lowest dielectric loss (0.02 at 1 kHz) and highest maximum working temperature (120 °C) in PVDF-based ferroelectric materials (dielectric loss: 0.03-0.05 for previously reported PVDF and copolymer films; 0.08-0.10 for terpolymer films; maximum working temperatures: 100-120 °C for previously reported PVDF and copolymer films; 50-60 °C for terpolymer films), which challenges the performance of commercial electrochemical capacitors and ceramic capacitors, with the added benefits of mechanical flexibility, toughness and low density.

Results

Pressed-and-folded PVDF for electric energy storage

Our approach uses a unique processing route called 'pressing-and-folding' (P&F), which draws inspiration from the process used by bakers to prepare puff pastry and croissants.[32] P&F is an iterative process in which the P&F cycle can be applied an arbitrary number of times (**Figure 1a**). Each P&F cycle is composed of a folding step, in which an approximately rectangular PVDF film, produced by hot pressing (HP), is folded, followed by a pressing and annealing step around the melting point (T_m) of PVDF (160-170 ˚C). For example (samples characterized in **Figure 1b**), the initial films (~50 mm×50 mm, thickness ~200 μm) were first folded and cold pressed with a compression force of 300 kN. The temperature was then increased from ambient temperature to 165 °C. The folded films were then held for 5 minutes under the conditions of

4

165 °C and 300 kN, followed by cold water quenching while maintaining the same compressive force. The maintenance of pressure during cooling was observed to facilitate the formation of β-phase (**Supplementary Figure 2**). During P&F, a fine and discrete layered structure is generated, with the thickness of each layer decreasing with the number of P&F cycles (Figure 1b). As expected, the initial HP films (no folding) contained predominantly α-phase, as confirmed by Fourier transform infrared spectroscopy (FTIR) (presence of characteristic peaks of α-phase at 764 cm^{-1}, 975 cm^{-1} and 1212 cm^{-1}, absence of the β/γ-characteristic peaks at 840 cm^{-1}) (**Figure 1c**).[33, 34] Surprisingly, P&F produced films containing about 98% of β-phase after seven P&F cycles (Figure 1c), higher than for any other reported method (max 85% by unidirectional/biaxial drawing, as highlighted by the horizontal green shaded area in Figure 1c).[16, 35, 36, 37, 38] The analysis of PVDF phase content has been well studied in previous research works[36, 37, 38], which includes the first determination of existing phases according to the appearance of exclusively characteristic bands (e.g. α-phase: 764 cm^{-1}, β-phase: 1275 cm^{-1} and γ-phase: 1234 cm^{-1} listed in **Supplementary Table 2**) and then calculation using specific equations based on the sample containing α- and β- phase only or containing a mixture of α-, β- and γ-phase. More details have been summarized in the **Supplementary Notes 1** in the SI. The folded samples show similar melting points compared to the initial HP materials (no folding) (**Supplementary Figure 3 and Supplementary Table 3**). The densities of films were measured based on the Archimedes principle, and are ~1.770 and 1.780 g cm^{-3} for HP and P&F samples, respectively. Consequently, the degree of crystallinity of HP and P&F samples are 41% and 38%, respectively, calculated using the densities of amorphous PVDF, pure α- and pure β-PVDF of 1.68, 1.92 and 1.97 g cm^{-3}, respectively.[39, 40] The calculated values of the degree of crystallinity are typical of PVDF.[41] For comparison, HP films were solid-state drawn to failure at 100 °C and 10 mm min^{-1}, which was reported to be the optimum conditions for obtaining the β-phase in a previous work,[35] achieving only ~65% of β-phase content (indicated by the blue dash line in Figure 1c) and a degree of crystallinity of 36% (density: 1.772 g cm^{-3}). The

ferroelectric hysteresis loops of the stretched films (thickness ~35 μm) could only be tested at relatively low electric fields (<350 kV mm^{-1}) due to the max limit of 10 kV applied voltage of our equipment (**Figure 1d**). From the schematic diagram of stored energy in ferroelectrics (Figure 1d), a lower remnant displacement (D_r), a higher maximum displacement (D_{max}) and a higher breakdown field (E_b) than the values found for the stretched films[31] would be favourable to obtain higher recoverable energy density U_{rec}. The P&F sample (one layer extracted from a film processed with seven P&F cycles, as described in section of materials and film preparation in Methods) showed an extremely high E_b, 880 kV mm^{-1}. The D_r and D_{max} are 0.017 and 0.144 C m^{-2}, respectively. All of these parameters contribute to a high U_{rec} of 35 J cm^{-3}, which is the highest value ever reported for any polymer-based dielectric capacitor. Despite the ultrahigh U_{rec}, the P&F samples also had higher energy efficiency η (~74%) compared to the stretched film (~54%) (Figure 1d). Moreover, the P&F films showed high breakdown strength with an average value of 789.5 kV mm^{-1}, as evaluated according to the criterion of Weibull distribution statistics (**Supplementary Figure 4**).

The above results raise two fundamental questions: why does P&F generate such a high content of β-phase (~98%)? And why do P&F films show relaxor-like ferroelectric behaviour?

Phase transformation from α- to β- during the P&F process

To answer the first question, we have investigated the dimensional changes of a sample during the P&F process (**Figure 2a**). The sample deformed plastically at each cycle, but its volume always remained constant according to the experiment results (Figure 2a). The maximum nominal stress (or pressure, **Figure 2b**) reached at the end of each cycle increases during the process as $P_i(n) = P_1 \left(\frac{2}{a}\right)^{n-1}$, where n is the number of cycles, P_1 is the pressure applied at the first cycle, and $a = 1.65$ (± 0.14) is a factor that describes how much the sample area increases during compression (**Supplementary Notes 2**). Atomic force microscopy (AFM) images

(**Figure 2c**) reveal the change of morphology during P&F, from spherulites (~2-3 µm in diameter) in the initial HP film to small granular structure (~150 nm in diameter) due to the increasing applied pressure with increasing number of P&F cycles.

The energy (Ω) that plastically deforms a unit volume of polymer provides the "driving force" for the phase transformation, and it grows with the number of cycles as $\Omega(n) = P_1(1-h)\frac{1-(2h)^n}{1-2h}$ (Supplementary Notes 2), where $h = 0.61$ ($\pm$ 0.09) is a factor that describes how much the sample thickness decreases during compression. Within this context, it is worth noting that the β-phase has a smaller unit cell volume (108.2 Å^3) compared to the α-phase (118.6 Å^3) for the same number of atoms.[11] Moreover, judging by the calculated values of intra- and inter-molecular potential energy, -6.03 kcal mol^{-1} and -5.73 kcal mol^{-1} for α- and β-phase, respectively, the β-phase is slightly energetically less stable.[42] The imposition of the ever increasing pressure P_i leads to a closer packing of the atoms and, as a result, a favoured β-phase with all-trans chain conformation. These considerations are supported by studies on phase transformation in solid-state drawn[43][44], solid-state compression[45] and rolling processed[46] PVDF films. The amount of β-phase (f_β) is proportional to Ω. Therefore, an advantage of the P&F process over the drawing process is that PVDF can always adsorb more "plastic energy" in compression than in tension.[47] Compression can be carried out in a broader (lower) temperature range than tension. Overall, the P&F process can allow higher phase conversions. Summarising, the increment of β-phase (Δf_β) depends on the increment of plastic energy ($\Delta\Omega$) adsorbed by the material, and must be limited by the amount of α-phase, i.e. by the term $1-f_\beta$, as when all the α-phase is converted there cannot be further increments of β-phase. From these considerations, and assuming that the fraction of β-phase before starting the P&F process is $f_{\beta 0}$ (8%), a differential calculation leads us to the following relationship between the amount of β-phase and plastic energy:

$$f_\beta(\Omega) = 1 - \left(1 - f_{\beta 0}\right)e^{-b\Omega} \tag{1}$$

or, in terms of P&F cycles,

$$f_\beta(n) = 1 - (1 - f_{\beta 0})e^{-c[1-(2h)^n]} \tag{2}$$

where b and $c = bP_1 \frac{1-h}{1-2h}$ are some proportionality constants. Figure 1c shows that the experimental data of f_β can be well fitted by Eq. 2 with $c=-1.1$, whereas the effects of different values of c on the β-phase amount during the P&F process is illustrated in **Figure 2d**. A number of factors should influence the relationship between f_β and Ω (i.e. the proportionality constant b, or c), as well as the amount of Ω that can be generated in the P&F process. We have tried to identify some of these factors, as it is clearly desirable to transform as much α-phase into β-phase possible with the lowest amount of plastic energy, or number of cycles.

First of all, the compressive stress-strain curve of PVDF is strain-rate dependent.[48] Therefore, for the same final nominal stress, the energy adsorbed depends on the final strain, hence there may be quicker phase conversion rates when pressing at different strain-rates. The second factor is the initial area (A_0) of the sample, a smaller A_0 corresponds to higher P_1, hence greater Ω. If A_0 is small enough, the pressure applied to the sample could be big enough to induce a total phase transformation in fewer cycles. **Figure 3a** shows the β-phase content of single-layer films (left-hand dataset) having different A_0 (25 cm^3, 4.5 cm^3 and 1 cm^3) after the initial pressure P_1; the film with the smallest A_0 allowed almost a complete phase transformation (95±5%) in just one cycle. Figure 3a shows also the importance of a third factor, the number of initial stacked layers constituting a film. At the same P_1, films made with six layers of hot pressed films (**Figure 3b**) presented much higher β-phase amounts than single-layer films. An explanation for this could lie in the friction between the PVDF and the hot-press platens. The friction induces shear-stresses that could dissipate energy[48] and reduce the pure elongation of the material in the plane perpendicular to the compression direction. Finite element method (FEM) simulations of film compression (**Figure 3c**) confirm that the internal layers of a multi-

layer structure can elongate and plastically deform more than the external layers, especially when the friction between the layers is smaller than the friction with the platens.

The two last important factors are the temperature of the annealing step (T_{anneal}) that follows the full closure of the hot-press and the molecular weight (M_{w}) of PVDF. They have a similar effect: lower T_{anneal} and higher M_{w} give lower chain mobility. **Figure 3d** presents the FTIR spectra of different M_{w} films annealed above their T_{m}; the β-phase increased more remarkably during the P&F process for higher M_{w} (>530 kg mol^{-1}) PVDFs. Moreover, in the low M_{w} (180 kg mol^{-1}) films also some γ-phase (chain conformation T_3GT_3G' **Figure 3e**) was produced. This is consistent with a previous work reporting α- to γ-phase transition in PVDF (M_{w} 180 kg mol^{-1}) under a minimal applied pressure of 200 kPa and a temperature range of 167-180 °C.[49] Apart from the M_{w}, the T_{anneal} plays a critical role; regardless of their M_{w}, all of the films presented only β-phase (>90%) when processed below their T_{m}, but maintained the non-polar α-phase when $T_{anneal} \gg T_{m}$ (Figure 3e and **Supplementary Figure 5**). More details on the factors influencing the phase transformation can be found in the Supplementary Notes 2.

Relaxor-like ferroelectric behaviour in P&F films

Having observed the formation of ultrahigh content of β-phase by P&F and proposed a possible mechanism, hereafter we focus on the ferroelectric behaviour of P&F PVDF films. The bipolar ferroelectric current-displacement-electric field (*I-D-E*) characteristics were measured under different electric fields at room temperature using a triangle waveform with a frequency of 10 Hz (**Figure 4**). It is noted that the *D-E* loops alone are insufficient to demonstrate ferroelectric properties and clarify the type of ferroelectric behaviour. Instead, it is more informative to study the raw *I-E* curves, in which the presence of ferroelectric domain switching peaks and/or field induced structure transition can easily be identified. Only some of the P&F samples with higher M_{w} polymers samples (534 and 670 kg mol^{-1}) showed relaxor-like ferroelectric behaviour[50] (**Figure 4a**), slim *D-E* loops with low D_{r} and high D_{max}. The M_{w} 180 kg mol^{-1} polymer samples

showed four current peaks located in the first and third quadrant at electric fields lower than 200 kV mm^{-1}, which merged into two current peaks at 300 kV mm^{-1} (Figure 4a), indicating the field-induced polar structural changes in P&F samples with low M_w (180 kg mol^{-1}). This is further proved by measuring the second ferroelectric hysteresis loops (**Supplementary Figure 6**) which differ from those obtained on pristine films (Figure 4a) and demonstrate that the above structural changes are not reversible. The higher M_w P&F samples (534 and 670 kg mol^{-1}) show four currents peaks located in all of the four quadrants (denoted as P_1, P_1', P_2 and P_2'in Figure 4a), which is related to the reversible field-induced polar structural changes. P_1 and P_1' correspond to the regulation of polar structures upon the application of electric field, and the appearance of P_2 and P_2' demonstrates that the polar structures can reverse back to the original state upon the remove of electric field, which is also proved by almost the same shape of re-measured hysteresis *I-D-E* loops (Supplementary Figure 6). Note that P_2 and P_2'shifted across y-axis with further increasing electric field up to 800 kV mm^{-1}, which makes the four current peaks locate in the first and third quadrant and highlights the existence of partial irreversible phase transition due to the influence of ultrahigh electric field.

Previous to P&F, PVDF was reported to show double hysteresis loops, but only at an extreme condition[51], -100 °C, 0.003 Hz, and 240 kV mm^{-1}, and more importantly, the regarding detailed studies of *I-E* loops were not presented. Zhu *et al* [52] also studied the ferroelectric hysteresis loops of e-beam irradiated PVDF-TrFE and PVDF-TrFE-based terpolymers, and concluded that pinning polymer chains makes the e-beam irradiated PVDF-TrFE show relaxor-ferroelectric narrow hysteresis loops and PVDF-TrFE-based terpolymers present double hysteresis loops, however, without the interpretation of *I-E* curves, the underlying physical mechanisms cannot be precisely decoded. The double hysteresis *D-E* loops can be produced by the phase transition between anti-ferroelectric to ferroelectric[53] and paraelectric to ferroelectric[54] with two completely different physics mechanisms. In literature, PVDF-TrFE with high content of TrFE (47/53 mol. % and 37/63 mol. %) and PTrFE materials were reported

to show four current peaks located in all four quadrants[55, 56] ($<$150 kV mm^{-1}), which is ascribed to the reversible field-induced structural change between the disordered trans phase (weak polar) and well-ordered all trans phase (strong polar), as supported by in situ XRD measurement with applied electric field, being consistent with our analysis for P&F PVDF.

X-ray diffraction (XRD) was conducted to gain further insight into the field-induced structural changes in the P&F samples (**Supplementary Figure 7**). The XRD data show a reduction of the mean size of the crystallites, from ~20 nm in the initial HP films to ~5 nm after the P&F treatment (**Supplementary Table 4**). The average size of the crystallites in the P&F samples decreased from 6 nm to 3.5 nm with increasing M_w from 180 to 670-700 kg mol^{-1} (Supplementary Table 4), which can be related to the reduced chain mobility with increasing M_w. In P&F films with low M_w, it is believed that relatively large-sized polar structures possess higher thermal stability.[57] The application of an external electric field will induce the re-orientation of CF$_2$ dipoles and cause the regularization of the polymer chains,[58] leading to a structural change to long-range ferroelectric order (schematic images in **Figure 4b**). In the P&F films with high M_w (534 and 670-700 kg mol^{-1}), the small-sized polar structures are not stable due to the randomization of polarization induced by thermal activation.[57] In this case, the polar structures remain relatively small, despite the influence of the external field (schematic images in Figure 4b). Consequently, a significant fraction of dipoles will reverse back upon decreasing the electric field, as evidenced by the much lower D_r, 0.020 C m^{-2} (Figure 4b), compared to 0.076 C m^{-2} in P&F with low M_w (Figure 4b). Consistently, the P&F samples with high M_w (670-700 kg mol^{-1}) exhibited lower piezoelectric d_{33} coefficients (-3.0/+4.2 compared to -10.8/+12.0 of P&F samples with low M_w of 180 kg mol^{-1}) after the ferroelectric measurement up to 300 kV mm^{-1}. No obvious piezoelectric resonance peak could be detected in the frequency dependence of the dielectric spectra of the poled 670-700 kg mol^{-1} P&F films, while a small but clear peak (thickness extension mode) can be seen for the poled 180 kg mol^{-1} P&F films (**Supplementary Figure 8**). This confirms the existence of readily reversible polar structures

in high M_w P&F films. At high temperatures, the small-sized polar structures in P&F samples suffer severe thermal fluctuation and become even more unstable, as highlighted by the temperature dependence of the dielectric permittivity (**Supplementary Figure 9**) and ferroelectric hysteresis loops measured at high temperatures (**Supplementary Figure 10**), where the dielectric constant showed a declining trend at temperatures above 50 °C and the disappearance of current peaks (P_1' and P_2') upon the removal of electric fields (>140 °C).

Discussion

In summary, we have demonstrated a facile, readily implementable and scalable process, press-and-folding (P&F), to produce PVDF with good ferroelectric properties. Only seven P&F cycles are needed to transform the non-polar α-phase PVDF into the predominantly ferroelectric β-phase PVDF (~98%). The formation of the β-phase is proposed to be a result of a pressure induced phase transformation, and importantly, more effective stress transfer during P&F. Moreover, studies of the ferroelectric behaviour revealed relaxor-like ferroelectricity in P&F PVDF films with high M_w (534 and 670-700 kg mol^{-1}), which is attributed to reversible field induced structural change induced by the thermally unstable small-sized polar structures, as suggested by the decreasing crystallite size (down to ~4 nm) after P&F. An ultra-high energy density of 35 J cm^{-3} was achieved at 880 kV mm^{-1} in a P&F PVDF film with M_w of 670-700 kg mol^{-1}, being the highest value ever reported for a polymeric dielectric capacitor and well beyond the value for commercial electrochemical capacitors (20-29 J cm^{-3}). This finding promises to have a significant impact on the field of pulse power applications and could produce a step change in the field of dielectric capacitors, so far limited by their low energy storage density.

Methods

Materials and film preparation

Polyvinylidene fluoride (PVDF) pellets or powders with different molecular weight (M_w) 180 kg mol^{-1} and 534 kg mol^{-1} were purchased from Sigma Aldrich Chemical Co. PVDF with M_w of 670-700 kg mol^{-}

[1] (Solef® 6020) was purchased from Solvay S.A. The initial hot pressed (HP) films with an average area of 5 cm×5 cm were prepared using a Collin hot press P300E (Germany) at 180 °C and 113 kN for 2 minutes followed by cold water quenching to room temperature. The initial films were first folded and cold pressed at 300 kN. The temperature was then increased from ambient temperature to 165 °C. The folded films were then held for 5 minutes under the conditions of 165 °C and 300 kN, followed by cold water quenching with the pressure maintained. The overall thickness of the P&F films increases with the number of P&F cycles. For instance, the films thickness increases from 250-350 μm for hot pressed film to 1.0-1.2 mm for films after seven cycles.

Microstructure characterization

Fourier transform infrared spectroscopy (FTIR) (Tensor 27, Bruker Optik GmbH, Ettlingen, Germany) and wide-angle X-ray diffractometry (XRD) with Cu/Kα radiation (wavelength 0.15418 nm) (X'Pert Pro, PANalytical, Almelo, The Netherlands) were used to characterize the crystalline structure of the samples. Thermal analysis was performed using differential scanning calorimeter (DSC) (DSC 25, TA Instruments, Asse, Belgium) with a heating/cooling rate of 10 ℃ min^{-1}. The degrees of crystallinity of films were determined via measuring the densities of samples based on the Archimedes principle. The densities of amorphous PVDF, pure α- and pure β-PVDF are 1.68, 1.92, and 1.97 g cm^{-3}, respectively.[39,] [40] The morphology of samples was characterized using a scanning electron microscopy (SEM) (FEI Inspect-F, Hillsboro, OR, USA) and atomic force microscopy (AFM) (NT-MDT, Ntegra systems, Russia). The AFM images were obtained using tapping mode and recorded horizontally from left up to right bottom at a scanning rate of 1 Hz with pixel scan of 256×256. Nanoprobe cantilevers (PPP-NCHR, Nanosensors, Neuchatel, Switzerland) designed for non-contact AFM mode were used to acquire images.

Functional properties characterization

The temperature and frequency dependence of dielectric properties were characterized using a LCR meter (4284A, Agilent, Santa Clara, CA) and Precision Impedance Analyser (4294A, Agilent, Santa Clara, CA), respectively. Unipolar and bipolar ferroelectric hysteresis loops were obtained on a ferroelectric tester (NPL, Teddington, UK) at room temperature using a triangle waveform with a frequency of 10 Hz. The tester can only generate a maximum voltage of 10 kV, which significantly

limits the field that can be applied to relatively thick specimens. This is particularly problematic as the thickness of P&F films increases with P&F cycles (1.0-1.2 mm). In order to obtain films of relatively low thickness (~10 μm) comparable to stretched films (~35 μm), a thin layer of PTFE release agent was sprayed on the film surface before each P&F cycle. This allowed the separation of an individual thin layer from the multilayer P&F films. The presence of PTFE did not significantly modify the overall crystalline content, crystalline phase and discharged energy density (**Supplementart Figure 11**). The two-parameter Weibull analysis was performed to study the characteristic breakdown strength E_b of the one single layer of P&F film after seven cycles,

$$P(E) = 1 - \exp[-(E/E_b)^\beta]$$

The E is the breakdown field of ten samples measured during the ferroelectric hysteresis test, E_b is characteristic breakdown strength at which the probability of dielectric breakdown is 63.2%, $P(E)$ is the statistic cumulative probability of dielectric breakdown and β is the parameter related to the reliability of films.

Finite element method (FEM) modelling

The commercial package Abaqus Standard 6.14 (Dassault Systemes) was used to conduct simulations for this study. In all simulations, the models were discretized with eight-node brick element with reduced integration (C3D8R). A static analysis with large deformation formulation was performed, the material behavior was captured using a NeoHookean material perfectly plastic after the yield point. Contact between surfaces employed the Coulomb model of friction. Symmetry planes were used for the model geometry.

Data availability

The authors declare that the data supporting the findings of this study are available within the article and its Supplementary Information files and also are available from the corresponding authors upon reasonable request.

References

1.	Hao X. A review on the dielectric materials for high energy-storage application. *Journal of Advanced Dielectrics* **03**, 1330001 (2013).
2.	Christen T, Carlen MW. Theory of Ragone plots. *J Power Sources* **91**, 210-216 (2000).
3.	Kousksou T, Bruel P, Jamil A, El Rhafiki T, Zeraouli Y. Energy storage: Applications and challenges. *Sol Energy Mater Sol Cells* **120**, 59-80 (2014).
4.	Sarjeant WJ, Zirnheld J, MacDougall FW. Capacitors. *IEEE Transactions on Plasma Science* **26**, 1368-1392 (1998).
5.	Yao Z*, et al.* Homogeneous/Inhomogeneous-Structured Dielectrics and their Energy-Storage Performances. *Adv Mater* **29**, 1601727 (2017).
6.	Burke A. R&D considerations for the performance and application of electrochemical capacitors. *Electrochim Acta* **53**, 1083-1091 (2007).
7.	Sun H, Fu X, Xie S, Jiang Y, Peng H. Electrochemical Capacitors with High Output Voltages that Mimic Electric Eels. *Adv Mater* **28**, 2070-2076 (2016).
8.	Dang Z-M, Yuan J-K, Yao S-H, Liao R-J. Flexible Nanodielectric Materials with High Permittivity for Power Energy Storage. *Adv Mater* **25**, 6334-6365 (2013).
9.	Horiuchi S, Tokura Y. Organic ferroelectrics. *Nat Mater* **7**, 357 (2008).
10.	Jiang J*, et al.* Polymer Nanocomposites with Interpenetrating Gradient Structure Exhibiting Ultrahigh Discharge Efficiency and Energy Density. *Adv Energy Mater* **9**, 1803411 (2019).
11.	Lovinger AJ. Ferroelectric Polymers. *Science* **220**, 1115-1121 (1983).
12.	Meng N*, et al.* Processing and characterization of free standing highly oriented ferroelectric polymer films with remarkably low coercive field and high remnant polarization. *Polymer* **100**, 69-76 (2016).
13.	Ribeiro C*, et al.* Electroactive poly(vinylidene fluoride)-based structures for advanced applications. *Nature Protocols* **13**, 681 (2018).
14.	Katsouras I*, et al.* The negative piezoelectric effect of the ferroelectric polymer poly(vinylidene fluoride). *Nat Mater* **15**, 78 (2015).
15.	Meng N, Zhu X, Mao R, Reece MJ, Bilotti E. Nanoscale interfacial electroactivity in PVDF/PVDF-TrFE blended films with enhanced dielectric and ferroelectric properties. *Journal of Materials Chemistry C* **5**, 3296-3305 (2017).
16.	Gomes J, Nunes JS, Sencadas V, Lanceros-Mendez S. Influence of the β-phase content and degree of crystallinity on the piezo- and ferroelectric properties of poly(vinylidene fluoride). *Smart Mater Struct* **19**, 065010 (2010).
17.	Wu J*, et al.* Perovskite Srx(Bi1−xNa0.97−xLi0.03)0.5TiO3 ceramics with polar nano regions for high power energy storage. *Nano Energy* **50**, 723-732 (2018).
18.	Zhang QM, Bharti V, Zhao X. Giant Electrostriction and Relaxor Ferroelectric Behavior in Electron-Irradiated Poly(vinylidene fluoride-trifluoroethylene) Copolymer. *Science* **280**, 2101 (1998).
19.	Bobnar V, Vodopivec B, Levstik A, Kosec M, Hilczer B, Zhang QM. Dielectric Properties of Relaxor-like Vinylidene Fluoride−Trifluoroethylene-Based Electroactive Polymers. *Macromolecules* **36**, 4436-4442 (2003).
20.	Xu H, Cheng ZY, Olson D, Mai T, Zhang QM, Kavarnos G. Ferroelectric and electromechanical properties of poly(vinylidene-fluoride–trifluoroethylene–chlorotrifluoroethylene) terpolymer. *Appl Phys Lett* **78**, 2360-2362 (2001).
21.	Guan F*, et al.* Confined Ferroelectric Properties in Poly(Vinylidene Fluoride‐co‐Chlorotrifluoroethylene)‐graft‐Polystyrene Graft Copolymers for Electric Energy Storage Applications. *Adv Funct Mater* **21**, 3176-3188 (2011).

22. Li W, Meng Q, Zheng Y, Zhang Z, Xia W, Xu Z. Electric energy storage properties of poly(vinylidene fluoride). *Applied Physics Letters* **96**, 192905 (2010).

23. Prateek, Thakur VK, Gupta RK. Recent Progress on Ferroelectric Polymer-Based Nanocomposites for High Energy Density Capacitors: Synthesis, Dielectric Properties, and Future Aspects. *Chemical Reviews* **116**, 4260-4317 (2016).

24. Qi L, Petersson L, Liu T. Review of Recent Activities on Dielectric Films for Capacitor Applications. *Journal of International Council on Electrical Engineering* **4**, 1-6 (2014).

25. Ren X, Meng N, Yan H, Bilotti E, Reece MJ. Remarkably enhanced polarisability and breakdown strength in PVDF-based interactive polymer blends for advanced energy storage applications. *Polymer* **168**, 246-254 (2019).

26. Tan Q, Irwin P, Cao Y. Advanced Dielectrics for Capacitors. *IEEJ Transactions on Fundamentals and Materials* **126**, 1153-1159 (2006).

27. Wang Y, Zhou X, Chen Q, Chu B, Zhang Q. Recent development of high energy density polymers for dielectric capacitors. *IEEE Transactions on Dielectrics and Electrical Insulation* **17**, 1036-1042 (2010).

28. Wu S*, et al.* Aromatic Polythiourea Dielectrics with Ultrahigh Breakdown Field Strength, Low Dielectric Loss, and High Electric Energy Density. *Advanced Materials* **25**, 1734-1738 (2013).

9. Zhang X, Shen Y, Shen Z, Jiang J, Chen L, Nan C-W. Achieving High Energy Density in PVDF-Based Polymer Blends: Suppression of Early Polarization Saturation and Enhancement of Breakdown Strength. *ACS Applied Materials & Interfaces* **8**, 27236-27242 (2016).

30. Zhang Z, Chung TCM. Study of VDF/TrFE/CTFE Terpolymers for High Pulsed Capacitor with High Energy Density and Low Energy Loss. *Macromolecules* **40**, 783-785 (2007).

31. Zhou X*, et al.* Electrical breakdown and ultrahigh electrical energy density in poly(vinylidene fluoride-hexafluoropropylene) copolymer. *Appl Phys Lett* **94**, 162901 (2009).

32. Santagiuliana G*, et al.* Breaking the Nanoparticle Loading–Dispersion Dichotomy in Polymer Nanocomposites with the Art of Croissant-Making. *ACS Nano* **12**, 9040-9050 (2018).

33. Martins P, Lopes AC, Lanceros-Mendez S. Electroactive phases of poly(vinylidene fluoride): Determination, processing and applications. *Progress in Polymer Science* **39**, 683-706 (2014).

34. Hu ZJ, Tian MW, Nysten B, Jonas AM. Regular arrays of highly ordered ferroelectric polymer nanostructures for non-volatile low-voltage memories. *Nat Mater* **8**, 62-67 (2009).

35. Meng N*, et al.* Crystallization kinetics and enhanced dielectric properties of free standing lead-free PVDF based composite films. *Polymer* **121**, 88-96 (2017).

36. Cai X, Lei T, Sun D, Lin L. A critical analysis of the α, β and γ phases in poly(vinylidene fluoride) using FTIR. *RSC Advances* **7**, 15382-15389 (2017).

37. Benz M, Euler WB. Determination of the crystalline phases of poly(vinylidene fluoride) under different preparation conditions using differential scanning calorimetry and infrared spectroscopy. *Journal of Applied Polymer Science* **89**, 1093-1100 (2003).

38. Li Y*, et al.* Multiple stage crystallization of gamma phase poly(vinylidene fluoride) induced by ion-dipole interaction as revealed by time-resolved FTIR and two-dimensional correlation analysis. *Polymer* **55**, 4765-4775 (2014).

39. Ameduri B. From Vinylidene Fluoride (VDF) to the Applications of VDF-Containing Polymers and Copolymers: Recent Developments and Future Trends. *Chemical Reviews* **109**, 6632-6686 (2009).

40. Hasegawa R, Takahashi Y, Chatani Y, Tadokoro H. Crystal Structures of Three Crystalline Forms of Poly(vinylidene fluoride). *Polymer Journal* **3**, 600-610 (1972).

41. Li M, *et al.* Revisiting the δ-phase of poly(vinylidene fluoride) for solution-processed ferroelectric thin films. *Nat Mater* **12**, 433-438 (2013).

42. Hasegawa R, Kobayashi, M., Tadokoro, H. Molecular conformation and packing of poly(viny1idene fluoride). Stability of three crystalline forms and the effect of high pressure. *Polym J* **3**, 591-599 (1972).

43. Siesler HW. Rheo-optical fourier-transform infrared spectroscopy of polymers. 9. Stretching-induced II(α)-I(β) crystal phase transformation in poly(vinylidene fluoride). *Journal of Polymer Science: Polymer Physics Edition* **23**, 2413-2422 (1985).

44. Sencadas V, Gregorio R, Lanceros-Méndez S. α to β Phase Transformation and Microestructural Changes of PVDF Films Induced by Uniaxial Stretch. *Journal of Macromolecular Science, Part B* **48**, 514-525 (2009).

45. Martín J, Zhao D, Lenz T, Katsouras I, de Leeuw DM, Stingelin N. Solid-state-processing of δ-PVDF. *Materials Horizons* **4**, 408-414 (2017).

46. Sharma M, Madras G, Bose S. Process induced electroactive β-polymorph in PVDF: effect on dielectric and ferroelectric properties. *PCCP* **16**, 14792-14799 (2014).

47. Chow TS. Stress–strain behavior of polymers in tension, compression, and shear. *J Rheol* **36**, 1707-1717 (1992).

48. Walley SM, Field JE. Strain rate sensitivity of polymers in compression from low to high rates. *DYMAT Journal* **1**, 211-227 (1994).

49. Kang SJ, *et al.* Localized Pressure-Induced Ferroelectric Pattern Arrays of Semicrystalline Poly(vinylidene fluoride) by Microimprinting. *Adv Mater* **19**, 581-586 (2007).

50. Martín J, *et al.* Relaxations and Relaxor-Ferroelectric-Like Response of Nanotubularly Confined Poly(vinylidene fluoride). *Chemistry of Materials* **29**, 3515-3525 (2017).

51. Furukawa T, Date M, Fukada E. Hysteresis phenomena in polyvinylidene fluoride under high electric field. *Journal of Applied Physics* **51**, 1135-1141 (1980).

52. Yang L, *et al.* Relaxor Ferroelectric Behavior from Strong Physical Pinning in a Poly(vinylidene fluoride-co-trifluoroethylene-co-chlorotrifluoroethylene) Random Terpolymer. *Macromolecules* **47**, 8119-8125 (2014).

53. Tan X, Ma C, Frederick J, Beckman S, Webber KG. The Antiferroelectric ↔ Ferroelectric Phase Transition in Lead-Containing and Lead-Free Perovskite Ceramics. *J Am Ceram Soc* **94**, 4091-4107 (2011).

54. Kan D, Anbusathaiah V, Takeuchi I. Chemical Substitution-Induced Ferroelectric Polarization Rotation in BiFeO3. *Adv Mater* **23**, 1765-1769 (2011).

55. Oka Y, Koizumi N, Murata Y. Ferroelectric order and phase transition in polytrifluoroethylene. *Journal of Polymer Science Part B Polymer Physics* **24**, 2059-2072 (1986).

56. Furukawa T, Takahashi Y. Ferroelectric and antiferroelectric transitions in random copolymers of vinylidene fluoride and trifluoroethylene. *Ferroelectrics* **264**, 81-90 (2001).

57. Woo J, Hong S, Min DK, Shin H, No K. Effect of domain structure on thermal stability of nanoscale ferroelectric domains. *Appl Phys Lett* **80**, 4000-4002 (2002).

58. Furukawa T. Ferroelectric Properties of Vinylidene Fluoride Copolymers. *Phase Transitions* **18**, 143-211 (1989).

Author contributions

N.M. and X.R. produced samples and carried out the measurements and contributed equally to this work. G.S., L.V., and H.Z. contributed with the modelling and mechanism of phase transformation. J.W. and H.Y. participated in the analysis of dielectric and ferroelectric properties. M.R and E.B. initiated and mentored the work. All authors contributed to the preparation of the manuscript.

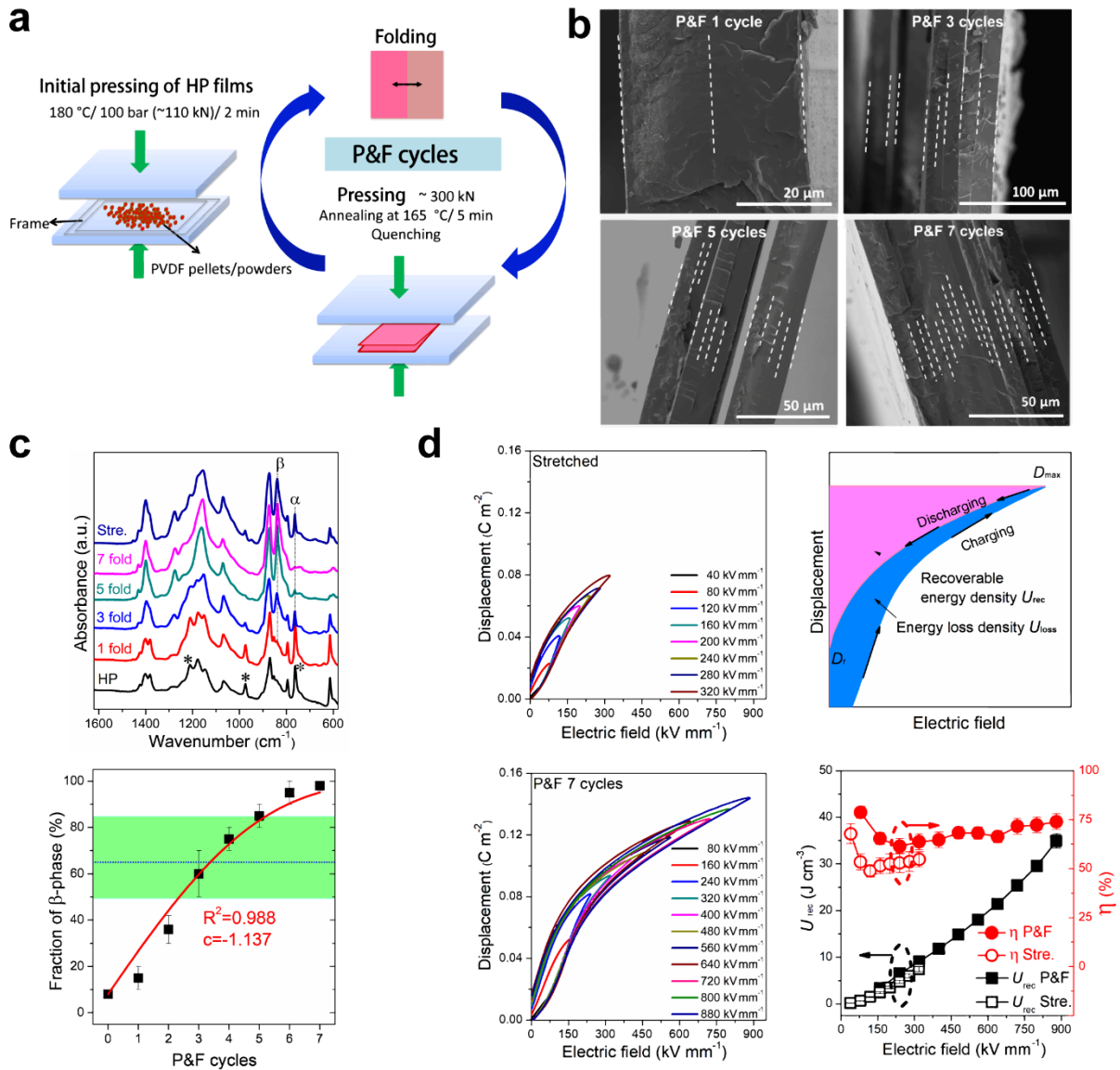**Competing interests**

The authors declare no competing interests.

Figures

Figure 1 PVDF (M_w=670-700 kg mol^{-1}) processed by P&F and a comparison with the stretched samples. (a) Schematic demonstration of P&F technique. (b) Cross-sectional SEM images of P&F samples folded at 165 °C and 300 kN after different numbers of folding cycles. A fine and discrete layered structure is generated during P&F. (c) The evolution of crystalline phases revealed by the FTIR absorbance spectrum. The initial hot pressed (HP) films mainly crystallized into α-phase with characteristic peaks at 764 cm^{-1}, 975 cm^{-1} and 1212 cm^{-1} highlighted by asterisks and transformed to about 98% β-phase (strong peak at 840 cm^{-1}) after seven folding cycles. The horizontal green shaded area indicates the reported values of fraction of β-phase in commonly stretched PVDF films, the blue dashed line represents the fraction of β-phase for the stretched film in this work, and the continuous line is the best fit of the experimental P&F data with Eq. 2 using c as free parameter ($f_{\beta 0}$ and h were set at 8% and 0.6, respectively). (d) A comparison of electric energy storage properties of P&F and stretched films, which includes ferroelectric hysteresis loops, schematic calculations of stored energy of ferroelectric materials and the recoverable energy density U_{rec} and energy efficiency η of P&F and stretched films.
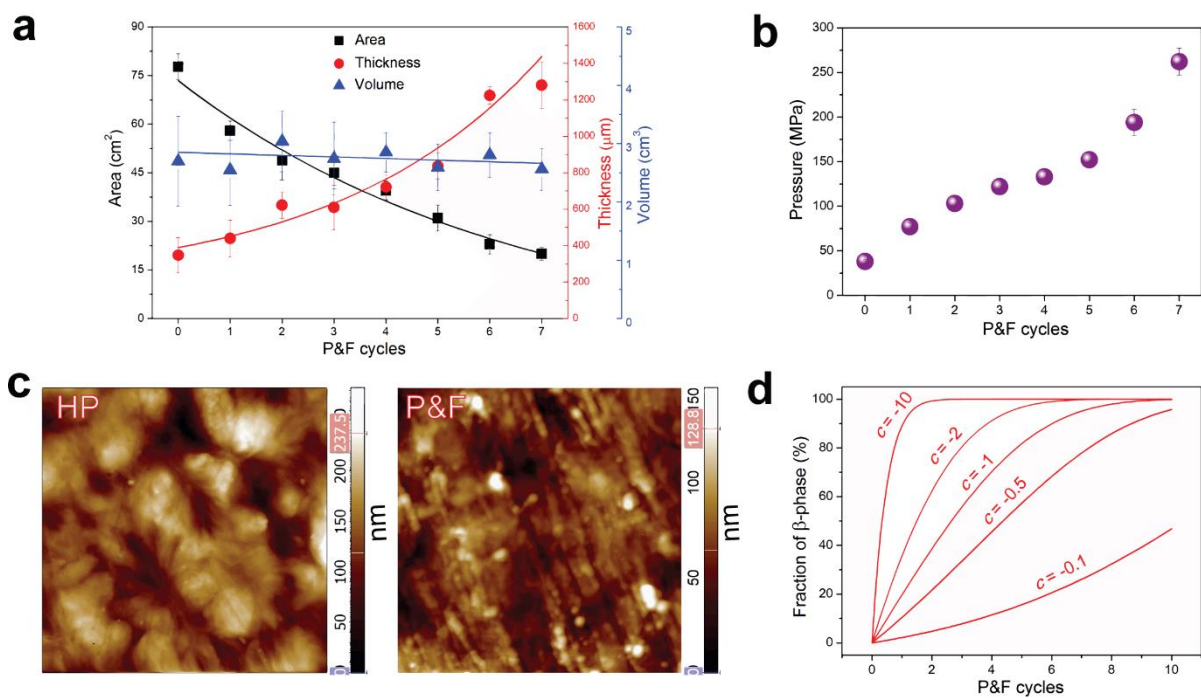
Figure 2 Morphological changes of PVDF samples (M_w=670-700 kg mol^{-1}) processed by P&F. (a) Variation of overall sample area, thickness and volume with the number of P&F cycles. (b) Calculated pressure (nominal stress) in purple data points for different P&F cycles. (c) AFM topography images (5 μm×5 μm) of initial HP (left) and P&F (right) after seven cycles, which show the evolution of morphology, from large spherulites in HP films to small granules after P&F films. (d) Theoretical changes of the β-phase content according to Eq. 2 with different values of parameter c.
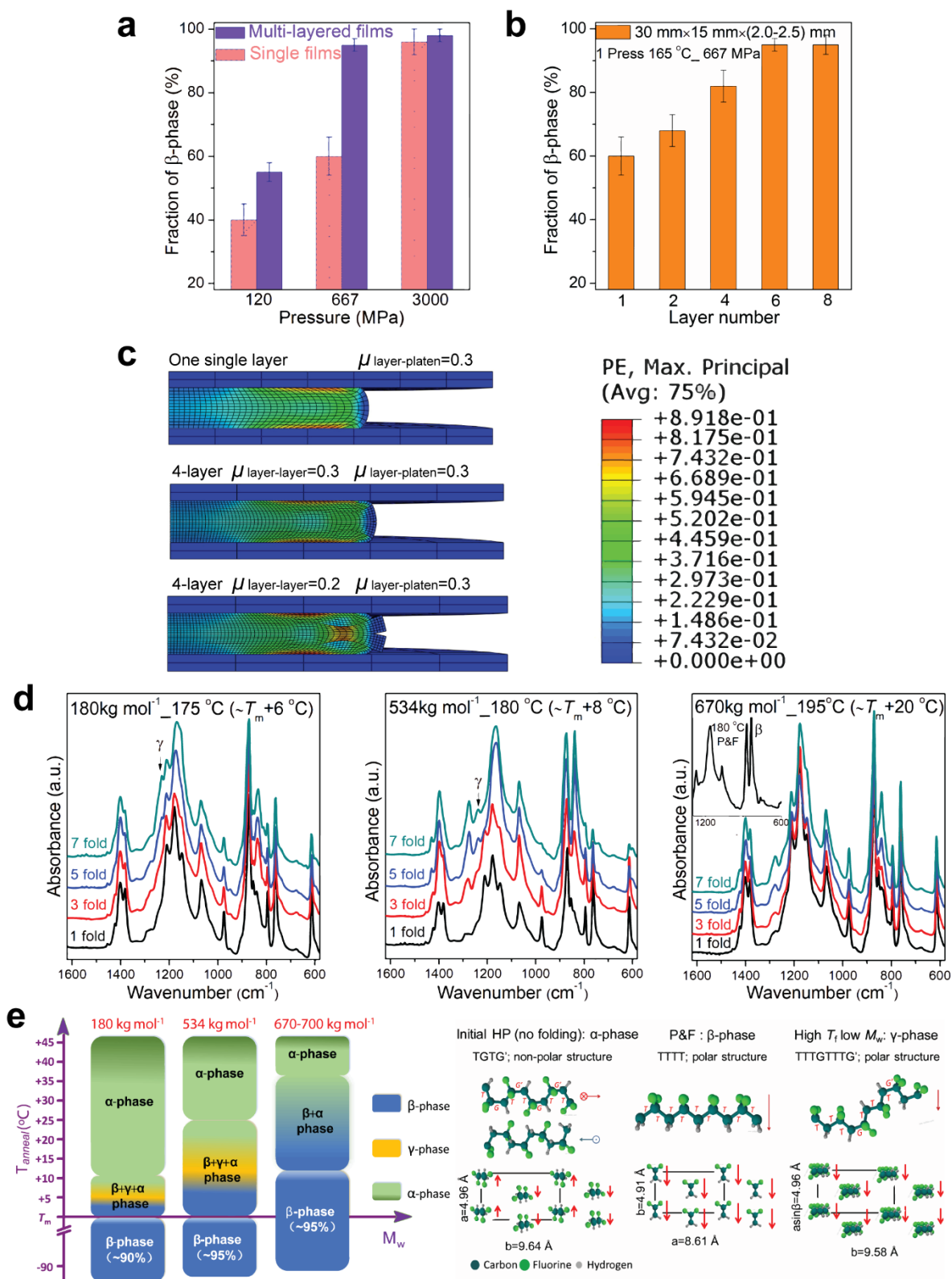
Figure 3 Factors influencing the formation of β-phase during P&F. (a) Comparison of the phase transition in samples (670-700 kg mol^{-1}) with mono-layer and six multi-stacked layers at three different pressures (force 300 kN), 120, 667 and 3000 MPa, followed by pressure-annealing at 165 °C for 5 minutes, which indicates that high pressure and layered structure favour the formation of β-phase. (b) Fraction of β-phase for samples (670-700 kg mol^{-1}) with the same dimensions but composed of different numbers of layers that were pressed once at 667

MPa (force 300 kN) followed by pressure-annealing at 165 °C for 5 minutes and cold water quenching. (c) FEM simulations of film compression in the cases of mono-layer film, 4-layer film with same friction coefficients μ between layer and platen and between layers, and 4-layer film with μ between layer and platen higher than μ between the layers. The bar scale represents the overall strain deformations. (d) FTIR of samples with different M_w, which indicates the formation of γ-phase in PVDF (low M_w) at higher T_{anneal} (denoted by the γ-characteristic band at 1234 cm^{-1}) and high M_w favours the transformation of β-phase (inset). For PVDF with M_w of 180, 534 and 670 kg mol^{-1}, T_m was 169, 172 and 172 °C, respectively. (e) Demonstration of phase evolution with T_{anneal} and M_w during P&F and schematic diagram of chain conformation, crystal structure and polarization of PVDF. The HP (no folding) films are mainly α-phase, with two trans-gauche-trans-gauche' (TGTG') chains anti-parallel packed in a pseudo-orthorhombic unit cell. The symbols and arrows represent the in-plane and out-of-plane contributions to the dipole moments. After P&F at different temperatures (room temperature to T_m), films formed into β-phase (>90 wt. %) with all-trans (TTT) chain conformation. Low T_{anneal} and high M_w favour the formation of β-phase.
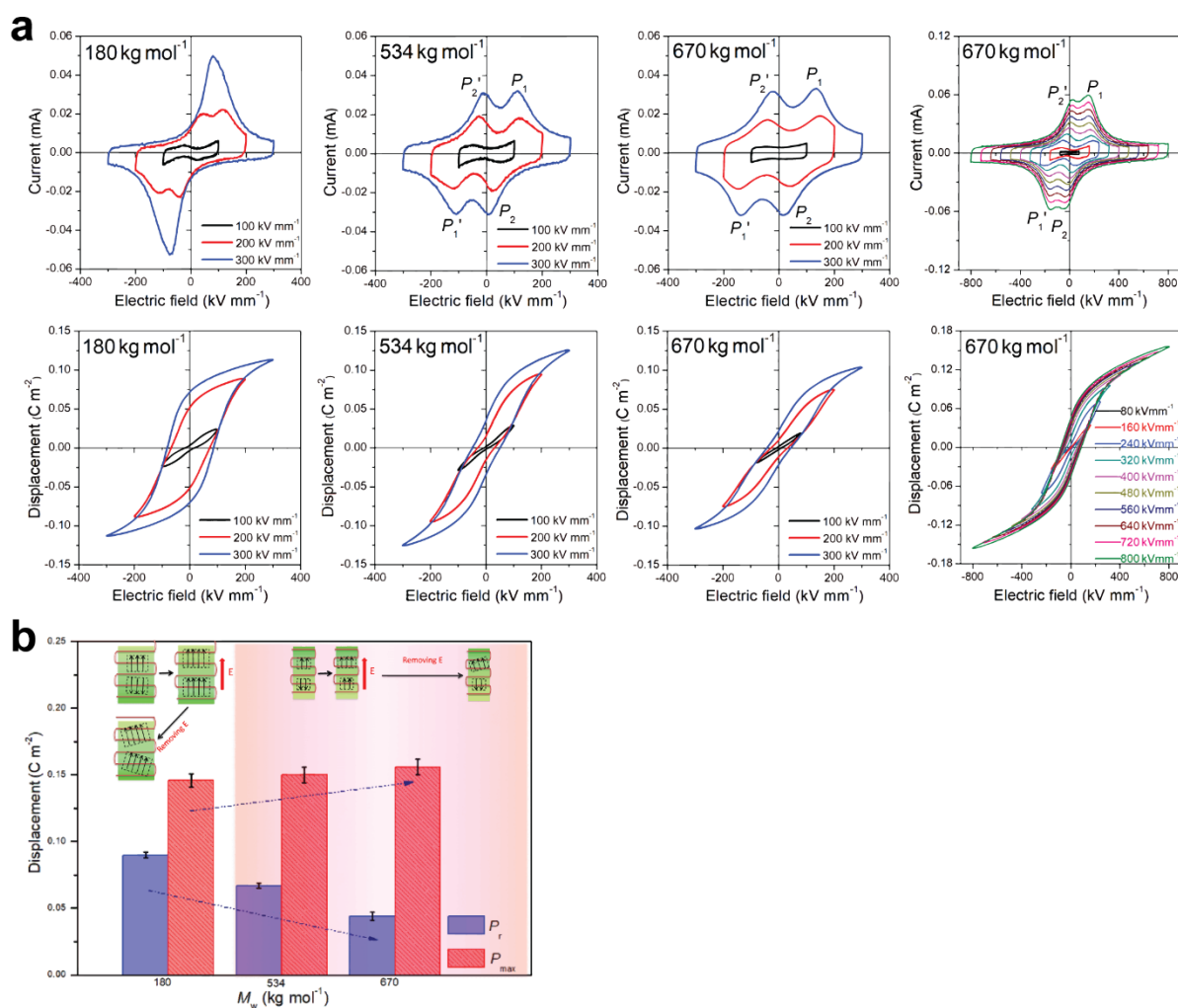
Figure 4 Ferroelectric properties of PVDF P&F samples. (a) Bipolar Current-Electric field (*I-E*) and Displacement-Electric field (*P-E*) of P&F PVDF after seven cycles with different M_w of 180 kg mol^{-1}, 534 kg mol^{-1} and 670 kg mol^{-1}. P_1 and P_1' denote the peaks appeared during the application of electric field. P_2 and P_2' denote the peaks appeared during the reversal of electric field. (b) A comparison of bipolar remnant polarization P_r and maximum polarization P_{max} of P&F films with different M_w, and schematic diagram of polar structure change during charging and discharging processes, where the green blocks represent the crystallites, red lines represent the polymer chains with arrows denoting the dipole moment, and the dashed lines highlight the polar structure, which was enhanced and grew larger under electric field.